Engineering Radial Deformations in Single-Walled Carbon and Boron Nitride Nanotubes Using Ultrathin Nanomembranes

Meng Zheng,[†] Lian-feng Zou,[†] Howard Wang,[†] Cheol Park,[‡,§] and Changhong Ke[†,*]

[†]Department of Mechanical Engineering, State University of New York at Binghamton, Binghamton, New York 13902, United States, [‡]National Institute of Aerospace, 100 Exploration Way, Hampton, Virginia 23666, United States, and [§]Department of Mechanical and Aerospace Engineering, University of Virginia, Charlottesville, Virginia 22904, United States

ABSTRACT Radial deformations of carbon and boron-nitride nanotubes are of great importance to their respective electronic properties and applications. In this paper, we present a simple and practical approach of engineering radial deformations in single-walled carbon and boron-nitride nanotubes (SWCNTs and SW-BNNTs) through covering individual nanotubes lying on flat substrates with subnanometer-thick monolayer graphene oxide (GO) nanomembranes. The GO membrane conforms to and transversely compresses the underlying nanotube as a result of its adhesion binding interaction with the substrate. Our atomic force microscopy (AFM) imaging measurements reveal that the engineered net radial deformations of both types of tubes increase with the tube diameter and are more for SW-BNNTs compared with SWCNTs of the same tube diameter. Our results capture the net cross-section height reductions of up to 44.1% for SW-BNNTs and up to 29.7% for SWCNTs. Our work clearly demonstrates the effectiveness of our proposed approach for engineering and controlling the radial deformation in one-dimensional tubular nanostructures and opens a promising route for mechanical tuning of their electronic properties for novel nanoelectronics applications.

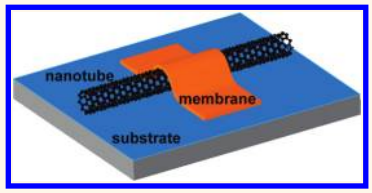

KEYWORDS: boron nitride nanotubes · carbon nanotubes · graphene-oxide nanosheets · radial deformation · atomic force microscopy

Radial deformations of one-dimensional tubular nanostructures, such as carbon nanotubes (CNTs) and boron-nitride nanotubes (BNNTs), are of great importance to their respective electrical properties and electronics applications (*e.g.*, field effect transistors (FETs),[1] single-electron transistors (SETs),[2] and optoelectronic devices[3]). From the structural point of view, CNTs and BNNTs are made of alike hexagonal sp2 covalent C−C and partially ionic B−N bonding networks, respectively. Both tubes have extraordinary mechanical and thermal properties. For instance, they have comparable Young's moduli, with reported values of up to 1.2−1.3 TPa.[4−10] Their thermal conductivities are reportedly to be above 3000 $W \cdot m^{-1} \cdot K^{-1}$.[11,12] However, the electrical properties of these two types of tubes are of distinct difference. Single-walled CNTs (SWCNTs) are either metallic or semiconductive depending on the tube chirality, while BNNTs are excellent insulators with band-gaps of about 5−6 eV and being largely independent of the tube chirality.[13−15] Both experiments and theoretical modeling demonstrate that the radial deformation of SWCNTs can greatly influence their electronic structures (*e.g.*, band-gaps) and result in semiconductor-to-metal or metal-to-semiconductor transitions in reportedly reversible fashions.[16−21] In addition, studies show that radial deformation can reduce the band gap of BNNTs from insulator to semiconductor or even conductor.[18,22] Tuning the band-gaps of these tubular nanostructures through engineering their transverse deformations will greatly impact many of their novel electronics applications.

Prior studies show that noticeable tube deformation occurs along its transverse direction when a carbon nanotube is deposited on a flat substrate, which is due to the van der Waal (vdw) interaction between the nanotube and the substrate.[23−25] However, such radial deformation is only substantial for nanotubes of very large diameters (*e.g.*, 4−5 nm). For SWCNTs of relatively small diameters, none-to-little radial deformation occurs. For instance, MD simulations show that vdw adhesion-induced radial deformation for a (20, 20) SWCNT (2.70 nm in diameter) is about 13% of its original tube

* Address correspondence to cke@binghamton.edu.

Received for review December 13, 2011 and accepted January 20, 2012.

Published online January 26, 2012
10.1021/nn2048813

© 2012 American Chemical Society

diameter, while merely 2% for a (10,10) tube of 1.34 nm in diameter.[23] It is noted that substantial radial deformations, as higher as 50% of the original tube diameter,[18,19] are desired for inducing significant band gap and electrical conductance changes in nanotubes. Significant radial deformations on individual tubes can be engineered using nanomanipulation with sharp scanning probe microscopy (SPM) probes.[2,21,26] However, this method is a slow and sequential approach, which is only useful for a very small quantity of nanotubes and is not feasible for large-scale processing. Introducing significant radial deformations in nanotubes with scalability for large-scale integration is still not available.

In this paper, we propose a simple and practical approach for engineering radial deformations in individual nanotubes, and demonstrate its effectiveness through engineering radial deformations in SWCNTs and single-walled BNNT (SW-BNNTs). Our proposed approach is to cover or partially cover individual nanotubes lying on flat substrates with subnanometer-thick nanomembranes, as illustrated in Figure 1a. Figure 1b shows schematically the cross sections of a nanotube with a height of h_0 (left) and the membrane-covered nanotube (right) staying on a flat substrate, respectively. The cross-section height of the membrane-covered nanotube, h, is measured as the height difference of the membrane from the position right on top of the underlying nanotube to the position of the flat covering of the substrate. The nanomembrane conforms to the underlying nanotube as a result of a balanced competition between the in-plane membrane rigidity and the adhesion interaction between the nanomembrane and the substrate/nanotube. Consequently, the nanomembrane imposes a compressive load to mechanically deform the underlying nanotube in its transverse direction. The radial deformation of the nanotube covered by the nanomembrane can be quantified by measuring parameters h and h_0. We choose monolayer graphene oxide (GO) sheet as the nanomembrane in our study mainly for the following factors: (1) the monolayer GO sheet is ~0.7 nm in thickness and readily conforms to the underlying nanotube in a relatively uniform fashion; (2) the GO sheet has a relatively high Young's modulus (E_{GO} = 207 GPa[27]), which has the advantage of inducing large compressive loads on the underlying nanotube; (3) the GO sheet is water-soluble and can be processed and patterned by existing micro/nanofabrication techniques;[28,29] (4) the GO sheet is electrically insulating[30] and does not directly interfere with the electron transport in the underlying nanotube. In addition, if desired, the GO sheet can also be readily reduced to graphene.[28,30,31] In this study, we investigate both the cross-section deformations of the GO sheet-covered individual SWCNTs and SW-BNNTs and the structural morphology of the covering monolayer GO sheets

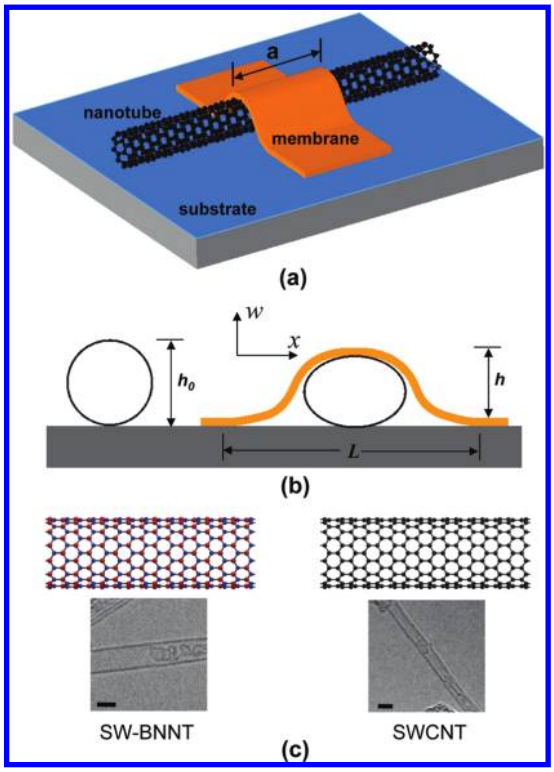

Figure 1. (a) Schematic of a nanotube on a flat substrate partially covered by a thin membrane: *a* is the length of the nanotube segment covered by the membrane. (b) Schematics of the cross sections of a nanotube (left) and a membrane-covered nanotube (right) on a flat substrate. (c) Schematic drawings and representative HRTEM images of SW-BNNTs and SWCNTs. Both tubes in the drawings are of zigzag (14, 0) chirality, in which the red, blue, and black dots represent nitrogen, boron, and carbon atoms, respectively. The scale bars represent 2 nm.

using atomic force microscopy (AFM) and nonlinear continuum mechanics theories. The schematics and representative high resolution transmission electron microscopy (HRTEM) images of both types of tubes are presented in Figure 1c. Our AFM measurements reveal that the engineered radial deformations for both types of tubes increase with the tube diameter, and are more for SW-BNNTs compared with SWCNTs of the same tube diameter. Our results capture net radial height reductions of up to 44.1% for SW-BNNTs and up to 29.7% for SWCNTs, which are substantially higher compared with the radial height reduction ascribed to the vdw interaction between the nanotube and the substrate. The observed difference in radial height reduction between SW-BNNTs and SWCNTs is ascribed to their difference in effective radial modulus.[32] Our results also reveal that the structural morphology of the covering monolayer GO sheet is governed by both membrane bending and stretching effects. The adhesion binding energy between monolayer GO sheets and flat SiO_2/Si substrates is found to be about 0.038 J/m^2. Our proposed approach of engineering radial deformations in nanotubes is compatible with existing micro/nano-fabrication techniques and thus suitable

for large-scale processing and integration. Our work contributes directly to the study of engineering and controlling the radial deformation of one-dimensional tubular nanostructures, and opens a promising route for mechanical tuning of their electronic properties for novel nanoelectronic applications.

RESULTS AND DISCUSSION

AFM Measurements of GO Sheet-Covered Nanotubes. Figure 2a shows a representative tapping mode AFM image of one GO sheet deposited on a silicon substrate. The measured height of the GO sheet is 1.5 ± 0.15 nm, which is consistent with the data reported in the literature about the monolayer GO sheet.[29,33,34] All the results and analysis presented in this paper are based on the monolayer GO sheets similar to the one shown in Figure 2a. Figure 2b shows one representative AFM image exhibiting three scenarios of GO sheet covered-CNTs, which are also observed for GO sheet-covered BNNTs. In this image, CNT #1 is partially covered by the GO sheet with only one tube end sticking out, CNT #2 is partially covered by the GO sheet in the central potion with both tube ends exposed, while CNT #3 is fully covered by the GO sheet. Both CNTs #1 and #2 are considered appropriate samples for our study because both h_0 and h can be directly measured, while only h can be measured for CNT #3. The uncovered tube cross-section heights (h_0) of CNTs #1 and #2 are measured to be 2.36 and 4.61 nm, respectively. Therefore, only CNT #1 may be a SWCNT (which is confirmed by our later analysis), while CNT #2 is most likely a multiwalled tube. The measured cross-section heights of CNT #1 in Figure 1b along its longitude direction are presented in the inset plot in Figure 2c, which displays a prominent transition around the edge of the GO sheet. The nanotube cross-section height varies on a very tight range (<0.5 Å) for both the uncovered and the GO sheet-covered portions away from the transition position, which can be ascribed to the variation of the tube diameter, the roughness of the substrate, and the noise in the AFM measurements. The red and blue curves in Figure 2c show the respective cross-section profiles of the uncovered and the GO sheet-covered portions of CNT #1 shown in Figure 1b based on the AFM-measured height data marked in the red and blue boxes. The tube height for the covered portion of this nanotube is measured to be h = 1.72 nm. Therefore, the tube height reduction as a result of the monolayer GO sheet covering is Δh = 0.64 nm. Similar tube cross-section height reduction because of the GO sheet covering is also observed on GO sheet-covered BNNTs. The CNT height profiles presented in Figure 2c are also contrasted with the respective cross-section profiles for one selected SW-BNNT of a similar original tube height. The measured cross-section height reduction for this BNNT is Δh = 0.74 nm, which is noticeably higher than that of the SWCNT of the same tube diameter. Such a difference

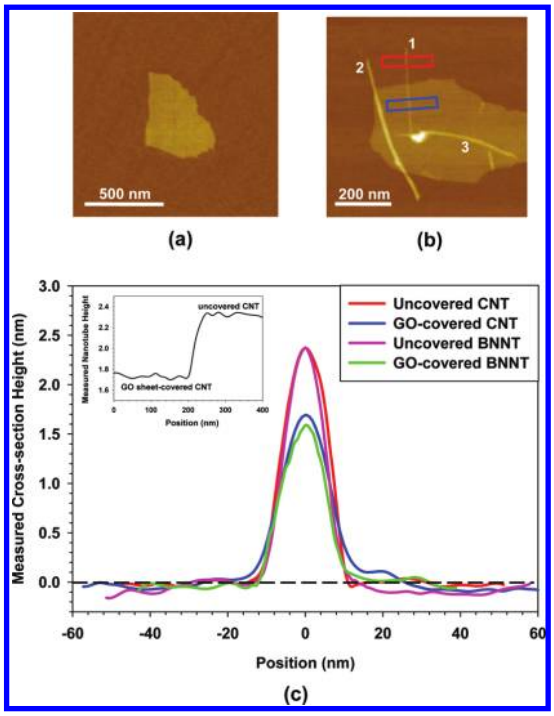

Figure 2. (a) AFM image of a monolayer graphene oxide (GO) sheet on a fresh silicon substrate. (b) AFM image of dispersed CNTs on a fresh silicon substrate covered or partially covered by a monolayer GO nanosheet. (c) Comparison of the respective cross-section profiles of the uncovered portion (red curve) and the GO-sheet-covered portion (blue curve) of CNT #1 shown in panel b. The pink and green curves are the respective cross-section profiles for one SW-BNNT of similar diameter to CNT #1 in panel b. The inset curve shows the variation of the measured tube height along the tube longitude axis for CNT #1 in panel b around the edge of the covering GO sheet.

in cross-section height reduction between GO-covered SW-BNNTs and SWCNTs are consistently observed on other measured samples. Figure 3a shows the dependences of the nanotube cross-section height reduction as a result of the monolayer GO sheet covering on the nanotube diameter based on measurements of 27 different SW-BNNTs and 15 different SWCNTs, whose original tube diameters are measured to be within 0.5 to 2.8 nm. The nanotube diameter here is defined as $D_{nt} = h_0 - t_{nt}$, in which t_{nt} = 0.34 nm is the interlayer distance of both the graphene and B−N sheets.[35,36] The key experimentally measured and theoretically predicted parameters on six selected GO-covered SWCNTs and SW-BNNTs are listed in Table 1.

Our results show that the measured radial height reduction for both types of tubes increases with the nanotube diameter. SW-BNNTs are found to consistently deform more in their transverse direction due to the GO sheet covering compared with SWCNTs of the same tube diameter. This result suggests that the radial rigidity of SW-BNNTs is lower compared with SWCNTs of the same diameter, which is consistent with our recently reported results on the effective radial moduli of SW-BNNTs and SWCNTs.[32] It is noted that

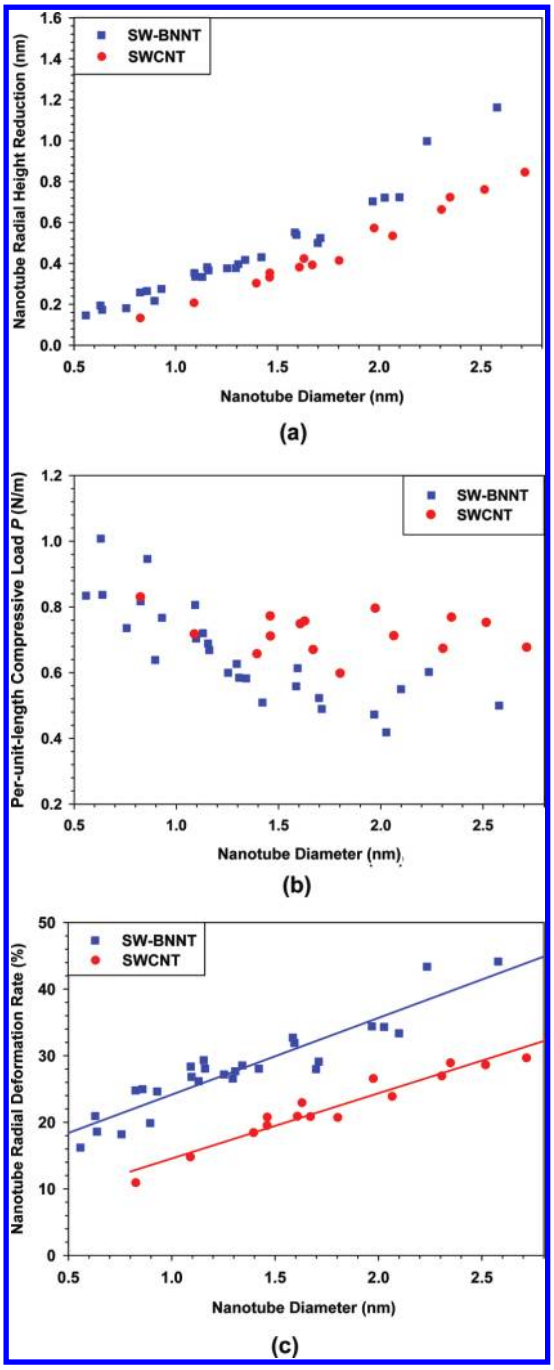

Figure 3. (a) The dependencies of the measured cross-section height reduction for SWCNTs and SW-BNNTs due to the covering of monolayer GO sheets on the nanotube diameter. (b) The respective per-unit-length compressive loads applied on SWCNTs and SW-BNNTs *versus* their tube diameters. (c) Comparison of the net radial deformation strain for SWCNTs and SW-BNNTs as a result of the covering of monolayer GO sheets. The solid lines are the linear-fitting curves of the respective experimental data sets.

double-walled (or even triple-walled) CNTs and BNNTs may also have their diameters within the diameter range shown in Figure 3a. However, such tubes have much higher radial rigidity compared with single-walled counterparts of the same outer diameter. Therefore, their radial height reduction due to the GO sheet covering is expected to be substantially lower compared with single-walled tubes, which is confirmed by our measurements (see Figure S1 in the Supporting Materials). In addition, we performed minimal cross-section height measurements on selected nanotubes to determine their tube-layer numbers based on the fact that the cross-section heights of highly compressed single-walled CNTs or BNNTs will be close to 0.68 nm (*i.e.*, twice of their interlayer distance values of 0.34 nm), while 1.36 nm for double-walled tubes and 2.04 nm for triple-walled tubes. The number of tube walls determined by our minimal cross-section height measurements is consistent with our analysis based on the data shown in Supporting Information, Figure S1. The detailed measurements of determining the number of tube layers in CNTs and BNNTs using this method will be reported in a separate publication.[37] Therefore, all the data shown in Figure 3a represent only SWCNTs and SW-BNNTs.

Radial Deformation of GO Sheet-Covered Nanotubes. Because the elastic modulus of GO sheets is much higher than the effective radial moduli of both SWCNTs and SW-BNNTs as well as the elastic modulus of the substrate (native oxide, 74 GPa), the deformation of the GO sheet along its thickness direction can be reasonably ignored. Therefore, the height reduction of the nanotube, $\Delta h = h_0 - h$, can be ascribed to the cross-section deformation of the nanotube and the deformation of the substrate. Since the AFM tip–sample interaction was controlled in the attractive force regime in the AFM tapping mode scanning process, the gentle contact of the AFM tip with the nanotube is not expected to result in any height reduction of the nanotube. Here, we reasonably assume that the mechanical deformations of the nanotube and the substrate are within the elastic regime, and therefore can be modeled using well-established contact mechanics theories. In our contact mechanics model, the GO sheet-covered nanotube is simplified as an elastic cylindrical body in contact with a flat substrate under a uniformly distributed compressive line load P. In our data analysis, the nanotube is assumed to undertake a circular cross-section on the substrate before being covered by the GO sheet, thus neglecting the effect of vdw interactions between the tube and the substrate on the flattening of the tube cross-section.[23] The combined nanotube–substrate deformation equals to the cross-section height reduction of the nanotube Δh and is given by[38]

$$\Delta h = P\left(\frac{1-\nu_{sub}^2}{\pi E_{sub}} + \frac{1-\nu_{nt}^2}{\pi E_{nt}}\right)\left[1+\log\left(\frac{2a^2}{\left(\frac{1-\nu_{sub}^2}{\pi E_{sub}} + \frac{1-\nu_{sub}^2}{\pi E_{sub}}\right)\cdot P\cdot h_0}\right)\right] \quad (1)$$

TABLE 1. List of the Key Experimentally Measured and Theoretically Predicted Parameters for Selected Monolayer GO Sheet-Covered SWCNT and SW-BNNT Samples

	D_{nt} (nm)	a (nm)	Δh (nm)	P (N/m)	ε_{nt}^{rad} (%)	L (nm) (theoretical-bending only)	L (nm) (theoretical-bending+stretching)	L (nm) (experimental)	M_0 (nN)	W_{flat} (J/m^2)
SWCNT #1	1.09	185	0.21	0.72	14.15	12.60	18.31	17.54	0.699	0.0400
SWCNT #2	1.46	165	0.33	0.77	18.88	13.07	20.64	23.70	0.717	0.0423
SWCNT #3	1.96	245	0.57	0.80	26.00	13.69	23.50	24.89	0.718	0.0423
SW-BNNT #1	0.83	225	0.26	0.82	13.10	10.91	14.11	16.09	0.787	0.0509
SW-BNNT #2	1.42	250	0.43	0.51	21.14	14.52	21.91	21.93	0.551	0.0249
SW-BNNT #3	1.97	170	0.70	0.47	29.31	15.84	26.10	23.76	0.512	0.0215

where E_{nt} and E_{sub} are the effective radial modulus of the nanotube and the Young's modulus of the substrate, respectively. ν_{nt} and ν_{sub} are the Poisson's ratios of the nanotube and the substrate, respectively. A native oxide layer of ~2 nm in thickness was measured on the surface of the Si substrates using ellipsometry (Model Uvisel, Horiba, Ltd.). The materials for the substrate are considered to be native silicon oxide with an elastic modulus of 74 GPa and a Poisson's ratio of 0.16. Poisson's ratios for SWCNTs and SW-BNNTs are assumed to be 0.17 and 0.2,[32] respectively. a is the length of the nanotube segment covered by the GO sheet, as illustrated in Figure 1a. The recently reported effective radial elastic moduli of both SW-BNNTs and SWCNTs[32] can be reasonably approximated as simple power functions of the tube diameter (D_{nt}), given by $E_{nt} = 13.428D_{nt}^{-2.203}$ (for SW-BNNTs) and $E_{nt} = 26.602D_{nt}^{-1.931}$(for SWCNTs), in which E_{nt} and D_{nt} are in units of GPa and nm, respectively.

The compressive load P is calculated using eq 1 for all the measured nanotubes shown in Figure 3a, and the results are presented in Figure 3b. For SW-BNNTs, P is found to be within the range of 0.4−1.0 N/m, displaying a decreasing trend with the increase in the tube diameter, while for SWCNTs, the calculated P is about 0.7 N/m and exhibits no appreciable dependence on the tube diameter. The net cross-section deformation of the nanotube δd can be estimated using eq 1 by considering the substrate as a rigid body. Figure 3c shows the dependence of the net nanotube radial deformation strain ε_{nt}^{rad}, defined as $\varepsilon_{nt}^{rad} = \delta d/d_{nt}$, on the tube diameter for both SW-BNNTs and SWCNTs. Our results reveal that ε_{nt}^{rad} increases, in nearly linear fashions, with the tube diameter for both types of tubes. SW-BNNTs are found to consistently deform more along their transverse directions than comparable SWCNTs, with the difference of about 10−15% in radial deformation strain within the measured tube diameter range. For SWCNTs, the net radial deformation strain is found to be about 18.4% for a tube of 1.4 nm in diameter and 29.7% for a tube of 2.7 nm in diameter, both of which are significantly higher than the previously reported radial strain values ascribed to the tube-substrate vdw interaction.[23] The net radial deformation strain reaches a remarkable value of 44.1% for a SW-BNNT of 2.6 nm in diameter. Our results clearly demonstrate that substantial nanotube cross-section flattening is produced as a result of covering individual nanotubes with monolayer GO sheets. We want to point out that the above-calculated net nanotube cross-section height reduction does not take into account the tube radial deformation induced by the vdw interaction between the tube and the substrate, which effectively results in an underestimation of the net nanotube radial height reduction and the corresponding strain rate. It is noted that the consideration of the vdw interactions among all the elastic bodies in our model requires advanced continuum and/or atomistic level modeling techniques (e.g., finite element methods and molecule dynamics simulations), which is beyond the scope of this study.

Structural Morphology of the Covering GO Sheet. The structural morphology of the GO sheet covered on top of the nanotube is of importance for understanding the compressive load applied on the nanotube and the adhesion interaction between the GO sheet and the substrate. It is noted that the substrate-regulated nanomembrane morphological deformations have recently been investigated based on monolayer graphene models using both continuum mechanics and molecular mechanics simulations.[39−43] In this study, the GO sheet is considered as a membrane with uniform thickness, and its cross-section deformation on top of the nanotube is theoretically modeled using continuum mechanics theory. With the consideration of both membrane bending and stretching effects, the in-plane deformation of the membrane, $w(x)$, is governed by

$$D_{GO}\frac{d^2w}{dx^2} = N\cdot w + M_0 - \frac{P}{2}\left(\frac{L}{2} - x\right) \qquad (2)$$

where $D_{GO} = (E_{GO}t^3)/(12(1 - \nu_{GO}^2))$ is the bending stiffness of the GO sheet in which E_{GO} = 207 GPa, t = 0.7 nm and ν_{GO} = 0.17 are the Young's modulus, thickness, and Poisson's ratio of the monolayer GO sheet, respectively. N is the stretching force in the membrane. L is the spanning width of the GO sheet (see Figure 1b). M_0 is the bending moment at $x = \pm L/2$. The boundary conditions for the deflected membrane include $w = dw/dx = 0$ at $x = \pm L/2$. It is noted that the

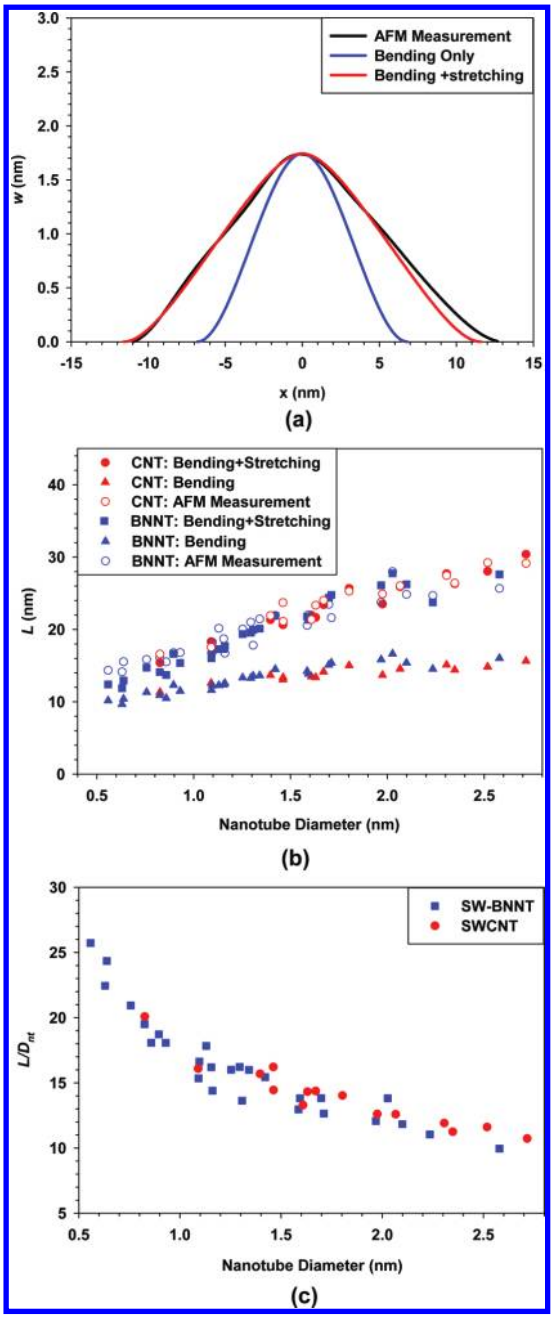

Figure 4. (a) The comparison of the experimentally measured and theoretically predicted cross-section morphological profiles of the GO-sheet on top of CNT #1 as shown in Figure 1b. The red curve represents the theoretical prediction based on the model considering both membrane bending and stretching effects, while the blue curve is based on the model considering only the membrane bending effect. (b) The dependencies of the experimentally measured and theoretically predicted GO sheet covering length L on the nanotube diameter for both SWCNTs and SW-BNNTs. (c) The dependencies of the ratio L/D_{nt} on the nanotube diameter D_{nt} based on the measured values L for both the tested SWCNTs and SW-BNNTs.

maximum deformation of the membrane $w(x = 0) = h$. Both the displacement of the GO sheet $w(x)$ and its spanning width L can be obtained using eq 2 based on the calculated line load P shown in Figure 3b. When the stretching force is neglected (*i.e.*, $N = 0$ in eq 2), the maximum deformation of the membrane due to pure membrane bending is given by $h = (PL^3)/(192D_{GO})$, and the deformation profile of the membrane is given by $w(x) = 4h[3(^1/_2 - {}^x/_L)^2 - 4(^1/_2 - {}^x/_L)^3]$ for $x \in [0, L/2]$. The deformation profile of the GO sheet covered on top of the nanotube is theoretically predicted for both scenarios (*i.e.*, membrane bending only *versus* both membrane bending and stretching). Figure 4a shows the comparison of the theoretically predicted deformation profiles for CNT #1 shown in Figure 2b and the experimentally measured profile by AFM. The radius of curvature (R_{tip}) of the employed AFM tips is estimated to be within 15−25 nm based on the geometrical deconvolution relationship $R_{tip} = \omega^2/8\Delta$, in which Δ and ω are the measured height and apparent width of a nanotube in the captured AFM images.[44] Because the radius of curvature of the employed AFM tip is much smaller than the radius of curvature of the deformed GO sheet, the AFM-measured GO sheet deformation profiles are free of the well-known tip−sample convolution artifacts. Our results shown in Figure 4a clearly reveal that the AFM-measured deformation profile of the GO sheet is in reasonably good agreement with the predicted deformation profile using eq 2 by considering both membrane bending and stretching effects. The measured GO sheet spanning width (L) using AFM is 24 nm, which is very close to the theoretically predicted value of 23 nm. It is noted that the theoretically predicted value of L using the model considering only the membrane bending effect is only 14 nm, indicating that the negligence of the stretching force in the membrane will substantially underestimate this quantity. Figure 4b shows the comparison of the theoretically predicted and experimentally measured spanning width of the GO sheet for all the tested nanotube samples, which consistently shows the good agreement on the GO sheet spanning width between the experimental measurements and the theoretically predicted values considering both the membrane bending and stretching effects. Figure 4c reveals that the ratios between the measured value of L and the nanotube diameter D_{nt} for all the tested SWCNTs and SW-BNNTs exhibit two decreasing and well-overlapping trends with the nanotube diameter. This observation suggests that the GO sheet wraps around the tube more tightly for tubes of larger diameters, which is consistent with the previously reported results on the wrapping configuration of graphene sheets around silicon nanowires on flat SiO_2 substrates obtained using continuum and molecular mechanics simulations.[39,43]

The Adhesion Energy between the GO Sheet and the Substrate. The adhesion interaction between the GO sheet and the substrate influences both the covering morphology of the GO sheet and the compressive load applied on the nanotube. The structural morphology of the GO sheet as shown in Figure 4a can be considered

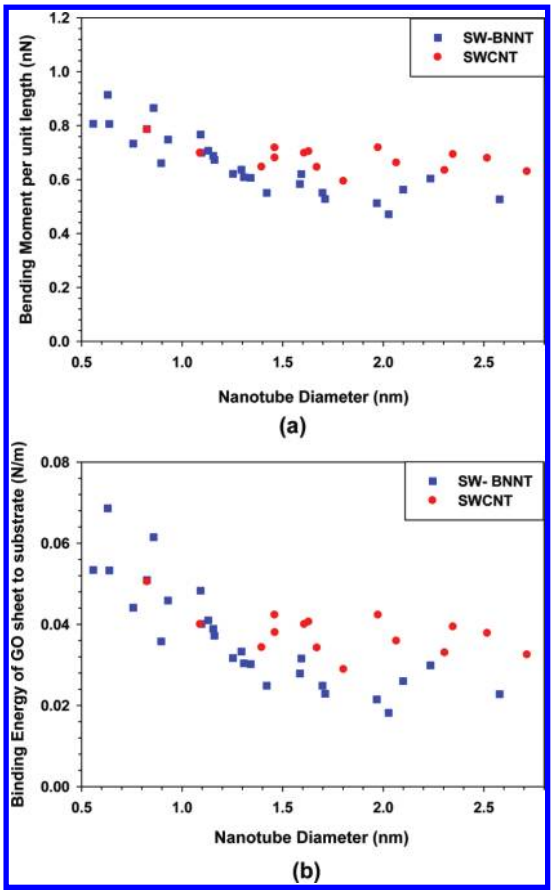

Figure 5. (a) The dependencies of the per-unit-length bending moment in the GO sheet at the delamination interface with the substrate on the nanotube diameter for both SWCNTs and SW-BNNTs. (b) The dependencies of the per-unit-area binding energy of the GO sheet to the substrate on the nanotube diameter based on the measurements for GO-covered SWCNTs and SW-BNNTs.

as a result of the delamination of the GO sheet from the substrate due to the existence of the underlying nanotube, which is ascribed to a balanced competition between the bending moment and the adhesion between the GO sheet and the substrate at the delamination front ($x = \pm L/2$). The reaction moment at the delamination front is equal to the bending moment in the GO sheet in the vicinity of the delamination front, that is, M_0. The adhesion energy per unit area or energy release rate at the delamination front is given by[45−47]

$$G = \frac{1}{2}\frac{M_0{}^2}{D_{GO}} \tag{3}$$

Figure 5a shows the calculated bending moment at the delamination front for both the tested SW-BNNTs and SWCNTs. Figure 5b shows the dependencies of the corresponding binding energy between the GO sheet and the substrate on the tube diameter. For GO sheet-covered SWCNTs, the average binding energy and the corresponding deviation is calculated to be 0.038 ± 0.005 N/m, while it is 0.037 ± 0.013 for GO sheet-covered SW-BNNTs. The binding energy for GO sheet-covered SW-BNNTs displays a decreasing trend with the increase in the tube diameter, while this trend is not appreciable for GO sheet-covered SWCNTs. It is important to highlight here that the adhesion energy between the GO sheet and the substrate is not only due to the long-range nonbonded van der Waals interaction between the GO sheet and the substrate, but also due to other factors such as the adhesion between the GO sheet and the nanotube and the residual humidity in the chamber where the experiments were performed. It is noted that our estimated value of the adhesion energy between monolayer GO sheets and silicon substrates with native oxide layers is substantially lower than the recently reported data regarding the adhesion energy between monolayer graphene sheets and SiO_2 substrates (0.15−0.45 J/m^2).[48,49] We argue that the functional groups on the basal graphene plane in the GO sheet increases the distance between the graphene basal plane to the substrate, thus significantly reducing the long-range nonbonded van der Waals interaction.

It is noted that the elastic modulus of monolayer GO sheets was obtained from stretching experiments based on a thickness value of 0.7 nm that was measured separately by AFM thickness tests.[27] Therefore, the calculated value of the bending stiffness (D_{GO}) may be overestimated because the bending stiffness of a thin plate is a cubic function of its thickness. While the inaccuracy in the value of D_{GO} will not have any material effect on our results regarding the radial deformation of the nanotube, it will affect the calculated deformational profile of the GO sheet and its binding energy with the substrate. Our analysis shows that the actual GO sheet spanning with L may be lower, while the binding energy G may be higher, than our reported values as a result of the possible overestimation of D_{GO}.

CONCLUSIONS

We investigate a new approach of engineering radial deformations in SWCNTs and SW-BNNTs using monolayer GO nanomembranes. By using a combined experimental−theoretical approach, we demonstrate that the GO sheet covering can induce substantial radial deformation in the underlying nanotube. Our results show that the radial deformation of the nanotube due to the GO sheet covering increases with the tube diameter and SW-BNNTs deforms more than SWCNTs of the same diameter. Our results capture net radial height reduction of up to 44.1% for SW-BNNTs and up to 29.7% for SWCNTs, which are significantly higher than the radial deformation induced purely by the vdw interaction between the nanotube and the substrate. The engineered substantial radial deformation in both carbon and boron nitride nanotubes is expected to have an influential impact on their electrical properties and thus their electronics applications. Since the GO sheet is water-soluble and can be

deposited and patterned on the substrate using well-established micro- and nanofabrication techniques, it is plausible that our proposed approach can be applicable for large-scale manipulation of the radial deformation and electrical properties of nanotubes, which can be useful for the development of large-scale nanoelectronic devices and nanoelectromechanical systems (NEMS).

EXPERIMENTS AND METHODS

The employed SWCNTs, purchased from Sigma-Aldrich Co. in the form of dried powders, were synthesized using chemical vapor deposition (CVD) methods. The employed SW-BNNTs were synthesized using pressurized vapor/condenser (PVC) methods.[35] The GO sheets were prepared following a previously reported method[50] and were measured to have a carbon-to-oxygen atomic ratio of 2.06 using X-ray photoelectron spectroscopy (XPS). The XPS measurements on the GO sheet samples were performed at room temperature and under ultrahigh vacuum conditions using a PHI 5000 VersaProbe instrument with monochromatic Al Kα X-rays at 1486.6 eV, a 200 μm diameter spot, and constant pass energy of 23.5 eV at a power of 50 W. Both CNTs and BNNTs were dispersed in aqueous solution using ultrasonication with the aid of ionic surfactant sodium dodecylbenzenesulfonate (NaDDBS).[32,37] The supernatant of the dispersed nanotube solutions was deposited on clean Si wafers using spin-coating, and was subsequently rinsed multiple times with deionized (DI) water to remove residue surfactants. The synthesized GO sheets dissolved in DI water were deposited on both clean Si wafers and Si wafers with dispersed nanotubes on top through spin-coating. All the GO sheet and GO sheet-covered nanotube samples were dried in an oven set at 90 °C for 12 h before AFM imaging measurements.

All AFM imaging measurements reported in this paper were performed using a Park Systems XE-70 AFM operating at room temperature inside a sealed chamber backfilled with dry nitrogen gas. The employed AFM is incorporated with a closed-loop feedback control feature in the *XYZ* axes. Tapping-mode AFM was performed with the tip−sample interaction controlled in the attractive force regime using silicon AFM probes (Applied Nanostructures, Inc.) with a nominal spring constant of 48 N/m and resonant frequency of 190 kHz. The fast scanning direction of the AFM tip was controlled to be perpendicular to the nanotube longitude axis, and only straight tubes are selected for the analysis. All AFM images were collected at a scan rate of 1.0 Hz, a scan line of 1024 × 1024 pixels, and scan sizes of 1000−2000 nm. The root-mean-square (rms) noise in the resonating amplitude of the AFM cantilever is measured to be 0.46 Å using the laser reflection scheme.

The high resolution transmission electron microscopy (HRTEM) characterization of CNTs and BNNTs was performed using a JEM 2100F TEM (JEOL Ltd.) operated at accelerating voltages of 120−200 kV.

Conflict of Interest: The authors declare no competing financial interest.

Acknowledgment. This work was funded by US Air Force Office of Scientific Research−Low Density Materials Program under Grant Nos. FA9550-11-1-0042 and FA9550-10-1-0451, and was also partially supported by the American Chemistry Society Petroleum Research Fund. We thank Dr. In-Tae Bae for his assistance with the TEM characterization. The XPS, the ellipsometry, and the HRTEM measurements were performed using the facilities in the Analytical and Diagnostics Laboratory at Binghamton University's Small Scale Systems Integration and Packaging Center (S^3IP).

Supporting Information Available: Additional data about the nanotube radial height reduction due to the covering of monolayer graphene oxide sheets for both BNNTs and CNTs. This material is available free of charge *via* the Internet at http://pubs.acs.org.

REFERENCES AND NOTES

1. Tans, S. J.; Verschueren, A. R. M.; Dekker, C. Room-Temperature Transistor Based on a Single Carbon Nanotube. *Nature* **1998**, *393*, 49–52.
2. Postma, H. W. C.; Sellmeijer, A.; Dekker, C. Manipulation and Imaging of Individual Single-Walled Carbon Nanotubes with an Atomic Force Microscope. *Adv. Mater.* **2000**, *12*, 1299–1302.
3. Chen, Z. G.; Zou, J.; Liu, G.; Li, F.; Cheng, H. M.; Sekiguchi, T.; Gu, M.; Yao, X. D.; Wang, L. Z.; Lu, G. Q. Long Wavelength Emissions of Periodic Yard-Glass Shaped Boron Nitride Nanotubes. *Appl. Phys. Lett.* **2009**, *94*, 023105.
4. Wei, X. L.; Wang, M. S.; Bando, Y.; Golberg, D. Tensile Tests on Individual Multi-walled Boron Nitride Nanotubes. *Adv. Mater.* **2010**, *22*, 4895–4899.
5. Chopra, N. G.; Zettl, A. Measurement of the Elastic Modulus of a Multi-wall Boron Nitride Nanotube. *Solid State Commun.* **1998**, *105*, 297–300.
6. Arenal, R.; Wang, M. S.; Xu, Z.; Loiseau, A.; Golberg, D. Young Modulus, Mechanical and Electrical Properties of Isolated Individual and Bundled Single-Walled Boron Nitride Nanotubes. *Nanotechnology* **2011**, *22*, 265704.
7. Hernandez, E.; Goze, C.; Bernier, P.; Rubio, A. Elastic Properties of C and $B_xC_yN_z$ Composite Nanotubes. *Phys. Rev. Lett.* **1998**, *80*, 4502–4505.
8. Suryavanshi, A. P.; Yu, M. F.; Wen, J. G.; Tang, C. C.; Bando, Y. Elastic Modulus and Resonance Behavior of Boron Nitride Nanotubes. *Appl. Phys. Lett.* **2004**, *84*, 2527–2529.
9. Golberg, D.; Costa, P. M. F. J.; Lourie, O.; Mitome, M.; Bai, X. D.; Kurashima, K.; Zhi, C. Y.; Tang, C. C.; Bando, Y. Direct Force Measurements and Kinking under Elastic Deformation of Individual Multiwalled Boron Nitride Nanotubes. *Nano Lett.* **2007**, *7*, 2146–2151.
10. Ghassemi, H. M.; Lee, C. H.; Yap, Y. K.; Yassar, R. S. Real-Time Fracture Detection of Individual Boron Nitride Nanotubes in Severe Cyclic Deformation Processes. *J. Appl. Phys.* **2010**, *108*, 024314.
11. Xiao, Y.; Yan, X. H.; Cao, J. X.; Ding, J. W.; Mao, Y. L.; Xiang, J. Specific Heat and Quantized Thermal Conductance of Single-Walled Boron Nitride Nanotubes. *Phys. Rev. B* **2004**, *69*, 205415.
12. Pop, E.; Mann, D.; Wang, Q.; Goodson, K.; Dai, H. J. Thermal Conductance of an Individual Single-Wall Carbon Nanotube above Room Temperature. *Nano Lett.* **2006**, *6*, 96–100.
13. Rubio, A.; Corkill, J. L.; Cohen, M. L. Theory of Graphitic Boron−Nitride Nanotubes. *Phys. Rev. B* **1994**, *49*, 5081–5084.
14. Blase, X.; Rubio, A.; Louie, S. G.; Cohen, M. L. Stability and Band-Gap Constancy of Boron−Nitride Nanotubes. *Europhys. Lett.* **1994**, *28*, 335–340.
15. Lee, C. H.; Xie, M.; Kayastha, V.; Wang, J. S.; Yap, Y. K. Patterned Growth of Boron Nitride Nanotubes by Catalytic Chemical Vapor Deposition. *Chem. Mater.* **2010**, *22*, 1782–1787.
16. Gulseren, O.; Yildirim, T.; Ciraci, S.; Kilic, C. Reversible Band-Gap Engineering in Carbon Nanotubes by Radial Deformation. *Phys. Rev. B* **2002**, *65*, 155410.
17. Kinoshita, Y.; Ohno, N. Electronic Structures of Boron Nitride Nanotubes Subjected to Tension, Torsion, and Flattening: A First-Principles DFT Study. *Phys. Rev. B* **2010**, *82*, 085433.
18. Kim, Y. H.; Chang, K. J.; Louie, S. G. Electronic Structure of Radially Deformed BN and BC_3 Nanotubes. *Phys. Rev. B* **2001**, *63*, 205408.

19. Shan, B.; Lakatos, G. W.; Peng, S.; Cho, K. J. First-Principles Study of Band-Gap Change in Deformed Nanotubes. *Appl. Phys. Lett.* **2005**, *87*, 2067697.
20. Crespi, V. H.; Cohen, M. L.; Rubio, A. *In Situ* Band Gap Engineering of Carbon Nanotubes. *Phys. Rev. Lett.* **1997**, *79*, 2093–2096.
21. Barboza, A. P. M; Gomes, A. P.; Archanjo, B. S.; Araujo, P. T.; Jorio, A.; Ferlauto, A. S.; Mazzoni, M. S. C.; Chacham, H.; Neves, B. R. A. Deformation Induced Semiconductor-Metal Transition in Single Wall Carbon Nanotubes Probed by Electric Force Microscopy. *Phys. Rev. Lett.* **2008**, *100*, 256804.
22. Bai, X. D.; Golberg, D.; Bando, Y.; Zhi, C. Y.; Tang, C. C.; Mitome, M.; Kurashima, K. Deformation-Driven Electrical Transport of Individual Boron Nitride Nanotubes. *Nano Lett.* **2007**, *7*, 632–637.
23. Hertel, T.; Walkup, R. E.; Avouris, P. Deformation of Carbon Nanotubes by Surface Van Der Waals Forces. *Phys. Rev. B* **1998**, *58*, 13870–13873.
24. Hertel, T.; Martel, R.; Avouris, P. Manipulation of Individual Carbon Nanotubes and Their Interaction with Surfaces. *J. Phys. Chem. B* **1998**, *102*, 910–915.
25. Tang, T.; Jagota, A.; Hui, C. Y. Adhesion between Single-Walled Carbon Nanotubes. *J. Appl. Phys.* **2005**, *97*, 074304.
26. Tombler, T. W.; Zhou, C. W.; Alexseyev, L.; Kong, J.; Dai, H. J.; Lei, L.; Jayanthi, C. S.; Tang, M. J.; Wu, S. Y. Reversible Electromechanical Characteristics of Carbon Nanotubes under Local-Probe Manipulation. *Nature* **2000**, *405*, 769–772.
27. Suk, J. W.; Piner, R. D.; An, J. H.; Ruoff, R. S. Mechanical Properties of Mono-layer Graphene Oxide. *ACS Nano* **2010**, *4*, 6557–6564.
28. Cote, L. J.; Cruz-Silva, R.; Huang, J. X. Flash Reduction and Patterning of Graphite Oxide and Its Polymer Composite. *J. Am. Chem. Soc.* **2009**, *131*, 11027–11032.
29. Robinson, J. T.; Zalalutdinov, M.; Baldwin, J. W.; Snow, E. S.; Wei, Z. Q.; Sheehan, P.; Houston, B. H. Wafer-Scale Reduced Graphene Oxide Films for Nanomechanical Devices. *Nano Lett.* **2008**, *8*, 3441–3445.
30. Gomez-Navarro, C.; Weitz, R. T.; Bittner, A. M.; Scolari, M.; Mews, A.; Burghard, M.; Kern, K. Electronic Transport Properties of Individual Chemically Reduced Graphene Oxide Sheets. *Nano Lett.* **2007**, *7*, 3499–3503.
31. Stankovich, S.; Piner, R. D.; Chen, X. Q.; Wu, N. Q.; Nguyen, S. T.; Ruoff, R. S. Stable Aqueous Dispersions of Graphitic Nanoplatelets *via* the Reduction of Exfoliated Graphite Oxide in the Presence of Poly(sodium 4-styrenesulfonate). *J. Mater. Chem.* **2006**, *16*, 155–158.
32. Zheng, M.; Chen, X.; Bae, I.-T.; Ke, C.; Park, C.; Smith, M. W.; Jordan, K. Radial Mechanical Properties of Single-Walled Boron Nitride Nanotubes. *Small* **2012**, *8*, 116–122.
33. Chen, C. M.; Yang, Q. H.; Yang, Y. G.; Lv, W.; Wen, Y. F.; Hou, P. X.; Wang, M. Z.; Cheng, H. M. Self-Assembled Free-Standing Graphite Oxide Membrane. *Adv. Mater.* **2009**, *21*, 3007–3011.
34. Pandey, D.; Reifenberger, R.; Piner, R. Scanning Probe Microscopy Study of Exfoliated Oxidized Graphene Sheets. *Surf. Sci.* **2008**, *602*, 1607–1613.
35. Smith, M. W.; Jordan, K. C.; Park, C.; Kim, J. W.; Lillehei, P. T.; Crooks, R.; Harrison, J. S. Very Long Single- and Few-Walled Boron Nitride Nanotubes *via* the Pressurized Vapor/Condenser Method. *Nanotechnology* **2009**, *20*, 505604.
36. DeBorde, T.; Joiner, J. C.; Leyden, M. R.; Minot, E. D. Identifying Individual Single-Walled and Double-Walled Carbon Nanotubes by Atomic Force Microscopy. *Nano Lett.* **2008**, *8*, 3568–3571.
37. Zheng, M.; Ke, C.; Bae, I.-T.; Park, C.; Smith, M. W.; Jordan, K. Radial Elasticity of Multi-walled Boron Nitride Nanotubes. *Nanotechnology* **2012**, in press.
38. Puttock, M. J.; Thwaite, E. G. *Elastic Compression of Spheres and Cylinders at Point and Line Contact*; Commonwealth Scientific and Industrial Research Organization: Melbourne, Australia, 1969.
39. Zhang, Z.; Li, T. Graphene Morphology Regulated by Nanowires Patterned in Parallel on a Substrate Surface. *J. Appl. Phys.* **2010**, *107*, 103519.
40. Li, T.; Zhang, Z. Substrate-Regulated Morphology of Graphene. *J. Phys: D-Appl. Phys.* **2010**, *43*, 075303.
41. Li, T.; Zhang, Z. Snap-through Instability of Graphene on Substrates. *Nanoscale Res. Lett.* **2010**, *5*, 169–173.
42. Aitken, Z. H.; Huang, R. Effects of Mismatch Strain and Substrate Surface Corrugation on Morphology of Supported Monolayer Graphene. *J. Appl. Phys.* **2010**, *107*, 123531.
43. Zhang, Z.; Li, T. A Molecular Mechanics Study of Morphologic Interaction between Graphene and Si Nanowires on a SiO_2 Substrate. *J. Nanomater.* **2011**, *2011*, 374018.
44. Gibson, C. T.; Watson, G. S.; Myhra, S. Scanning Force Microscopy—Calibrative Procedures for 'Best Practice'. *Scanning* **1997**, *19*, 564–581.
45. Ke, C.; Zheng, M.; Zhou, G.; Cui, W.; Pugno, N.; Miles, R. N. Mechanical Peeling of Free-Standing Single-Walled Carbon Nanotube Bundles. *Small* **2010**, *6*, 438–445.
46. Zheng, M.; Ke, C. H. Elastic Deformation of Carbon-Nanotube Nanorings. *Small* **2010**, *6*, 1647–1655.
47. Ke, C. H.; Zheng, M.; Bae, I. T.; Zhou, G. W. Adhesion-Driven Buckling of Single-Walled Carbon Nanotube Bundles. *J. Appl. Phys.* **2010**, 107.
48. Koenig, S. P.; Boddeti, N. G.; Dunn, M. L.; Bunch, J. S. Ultrastrong Adhesion of Graphene Membranes. *Nat. Nanotechnol.* **2011**, *6*, 543–546.
49. Zong, Z.; Chen, C. L.; Dokmeci, M. R.; Wan, K. T. Direct Measurement of Graphene Adhesion on Silicon Surface by Intercalation of Nanoparticles. *J. Appl. Phys.* **2010**, *107*, 026140.
50. Hummers, W. S.; Offeman, R. E. Preparation of Graphitic Oxide. *J. Am. Chem. Soc.* **1958**, *80*, 1339–1339.